Journal of Public Transportation Community
Vol. 6 No. 2, October 2026, pp. 63-96
Online: https://ejournal.poltekbangsby.ac.id/index.php/jptc/about
e-ISSN :2808-3393

Gain–Temperature Relationships in Microstrip Antenna Arrays: An Interim Scoping Review of Mechanisms, Measurement Approaches, and Evidence Gaps for Planar 2 × 4 Arrays

Teguh imam Suharto[1,*], Achmad Setiyo Prabowo[2], Ade Irfansyah[3], Yuyun Suprapto[4], Bambang Bagus Harianto[5], Nyaris Pambudiyatno[6], Graca Delidia M.M.Soares[7]

Air Navigation Engineering, Surabaya Aviation Polytechnic
Indonesia, Air Navigation Administration of Timor-Leste
Correspondence author: Teguh imam Suharto, teguhimamsuharto@poltekbangsby.ac.id, Surabaya, Indonesia,

Abstract

Microstrip antenna arrays are used in communication, radar, space, and heating applications, but "temperature" denotes different physical conditions. This scoping review mapped mechanisms, measurement approaches, and evidence gaps linking antenna gain and thermal behaviour, with attention to planar 2 × 4 arrays. A 366-record Scopus seed export was deduplicated and screened; nine supplied full-text reports were assessed against prespecified criteria and charted for geometry, gain or radiation metrics, power reference, thermal compartment, boundary conditions, validation, and 2 × 4 applicability. Five reports were provisionally eligible: two provided array-level gain-thermal evidence and three provided supporting material or qualification evidence. Hot-state simulation, post-exposure testing, material thermal cycling, and coupled electromagnetic-thermal modelling represented distinct pathways. No supplied eligible report directly validated a planar 2 × 4 gain-temperature relationship or populated the external-medium heating theme. The evidence indicates that gain should not be treated as a heat metric; interpretation requires matched power, exposure geometry, thermal object, and heat-transfer conditions. The review remains interim because full-text retrieval and independent dual-reviewer confirmation are incomplete.The principal contribution is a mechanism-based framework and a set of validation requirements for future planar 2 × 4 experiments; the findings apply only to the nine full texts assessed.

Keywords: microstrip antenna array, antenna gain, electromagnetic-thermal coupling, temperature measurement, scoping review

Article History:
Received: 4 June 2026 ; Reviewed : 18 June 2026; Accepted: 23 July 2026; Published : 1 October 2026
DOI: 10.46491/jptc.v6i2.2866

How to cite : Suharto, T. I., Prabowo, A. S., Irfansyah, A., Suprapto, Y., Harianto, B. B., Pambudiyatno, N., & Soares, G. D. M. M. (2026). Gain–Temperature Relationships in Microstrip Antenna Arrays: An Interim Scoping Review of Mechanisms, Measurement Approaches, and Evidence Gaps for Planar 2 × 4 Arrays. *Journal of Public Transportation Community*, 6(2), 63–96. https://doi.org/10.46491/jptc.v6i2.2866

© 2026 by the authors. Submitted for possible open access publication under the terms and conditions of the Creative Commons Attribution Share Alike (CC BY-SA) license (**https://creativecommons.org/licenses/by-sa/4.0/**)

INTRODUCTION

Background and Related Evidence

Microstrip antenna arrays are attractive in radar, communications, navigation, sensing, and space systems because aperture synthesis can increase directional gain while preserving a low-profile planar form. Thermal conditions, however, alter the same materials, dimensions, interfaces, and feed networks that establish radiofrequency performance. A 4 × 4 wideband patch array has been reported with a measured peak gain of 18.7 dBi at 15.5 GHz and computational assessment across −50 to 150 °C, illustrating that high gain and thermal robustness are related design concerns rather than interchangeable outcomes (R. Li et al., 2023). High-temperature navigation arrays extend the issue to more severe environments: an aluminum-alloy and ceramic Beidou array was designed for operation up to 400 °C, with the emphasis on retaining navigation-band radiation performance rather than on heating the surrounding air (F. Xu & Zhang, 2025). A conformal ceramic array exposed to 600 °C further demonstrates the importance of separating thermal treatment from in-situ radiofrequency measurement; in that study the reported prototype gain comparison was performed after cooling, whereas the hot condition was represented numerically (P. Li et al., 2026).

Material development broadens this electromagnetic-thermal problem. Printed satellite arrays have combined prototype radiofrequency tests with thermal cycling of printed structures and interconnections, but those qualification tests are not equivalent to a continuous gain-versus-temperature experiment on the complete antenna (Yoo et al., 2025). Low-permittivity $LiMSiO_4$ ceramics with thermal conductivity above 6 W m−1 K−1 have been proposed as microwave substrates and demonstrated in a simulated 36 GHz, 4 × 8 array, again separating material characterization from device-level thermal validation (W. Wang et al., 2025). Modified bismaleimide-triazine composites have likewise combined low dielectric loss and improved heat transport with a 2 × 2 array demonstration, while the thermal tests and the array tests remain distinct levels of evidence (H. Wang et al., 2026). Graphene-clad laminate provides another example: vacuum-assisted hot pressing markedly raises film conductivity and enables a 26 GHz flexible array, yet the processing temperature is a manufacturing condition, not evidence that antenna operation warms the environment (Song et al., 2020).

The literature also contains genuinely coupled or integrated thermal problems. ETC-Net predicts gain patterns and array-surface temperature distributions for square patch arrays from 2 × 2 to 5 × 5, linking the domains through a learned surrogate trained on multiphysics numerical data rather than through a controlled physical gain intervention (Jia et al., 2025). A compact 26.5 GHz 2 × 2 subarray has been packaged with a beamforming circuit and thermal-management structure, with simulations showing a reduction in reported peak temperature while active receiving gain is characterized at system level (R. Liu et al., 2026). System-in-antenna concepts similarly combine radiation, shielding, circuitry, and heat removal; one reported architecture reduces a package temperature while reporting a high integrated system gain, but this does not isolate passive antenna gain as the thermal cause (Ge et al., 2025). Earlier phased-array integration work embedded 52 radiating patches, transmitting modules, and microchannel heat sinks in one multilayer structure, demonstrating that beam scanning and heat transport can be co-designed without assuming that one scalar gain value determines temperature (Zhou et al., 2019).

A different evidence stream examines electromagnetic energy delivered to an external medium. A 2.45 GHz microstrip array used for wind-turbine de-icing produces a reported 13.9 dB gain while infrared observations vary coating composition, input power, distance, and irradiation duration; the temperature response therefore belongs to the exposed material and its exposure conditions (Y. Xia et al., 2026). Numerical work combining 2 GHz and 28 GHz sources shows that thermal diffusion changes how absorbed-energy patterns combine, so local power deposition and final temperature are not spatially identical quantities (Miura et al., 2021). A hemispherical 2 × 4 microstrip arrangement for hyperthermia reports a focal temperature of 44.8 °C under a 90 W condition, but that evidence concerns controlled heating of a phantom-oriented target rather than warming of unrestricted ambient air (Zhang et al., 2026). Millimetre-wave anatomical modelling likewise demonstrates that source distance, beam arrangement, and body geometry shape exposure distributions beyond what can be inferred from gain alone (Diao & Hirata, 2023).

Geometry and application context further limit direct transfer. An all-metal 4 × 2 X-band phased array combines beam steering and electronics cooling, but its radiator, materials, and packaging are not equivalent to a planar microstrip 2 × 4 array even though both contain eight radiating positions (Banerjee et al.,

2022). Multiphysics optimization of a CubeSat stacked antenna reports relatively stable gain over a broad thermal interval while impedance behaviour changes, illustrating why gain, matching, and structural deformation should be charted separately (Simone et al., 2021). A cordierite 2 × 2 array subjected to 500 °C exhibits a reported resonance shift and strong circularly polarized gain, yet the available evidence does not establish a complete in-situ gain sweep through temperature (Pramono et al., 2025). Hybrid ceramic packaging at 15 GHz similarly links thermal-resistance motivation with a 2 × 2 array demonstration, without providing a direct gain-temperature response (Myllymäki et al., 2022). A 4 × 1 Ku-band array with metamaterial loading and protective superstrates reports gains around 12 dBi and good simulation-measurement agreement, while thermal protection remains an intended function rather than a controlled temperature-sweep result in the supplied full text (Desouky et al., 2026).

These distinctions matter because the phrase "gain-temperature relationship" can represent several physically different directions. A graphene-oxide absorber study explicitly links energy absorption, temperature, and antenna characteristics, showing how a thermally responsive material can change the radiating system (Rani et al., 2020). Cryogenic characterization of a superconducting microstrip array places the antenna in a controlled low-temperature measurement environment, making temperature an imposed condition on radiation performance (Zeng et al., 2017). Conversely, the term low-temperature co-fired ceramic denotes a fabrication technology and does not, by itself, demonstrate operational thermal testing; an active K-band antenna-in-package can report large system gain without establishing a passive gain-temperature relationship (Zhao et al., 2025). Reviews of 5G and 6G base-station cooling therefore treat thermal management as a system problem involving heat generation, transport paths, packaging, and boundary conditions rather than as a consequence of antenna gain alone (Dbouk & Mourad, 2025). Spaceborne-array studies that couple thermal, structural, and electromagnetic models reach the same general methodological need: thermal loading changes geometry and material state, and the resulting radiofrequency response must be traced through an explicit multiphysics chain (Fan et al., 2025).

Studies cited in this section and in Section 3.5 other than the five provisionally eligible reports (Tables 1–5) serve as contextual literature only; they

do not contribute to the eligibility accounting or to the evidence codes reported in Section 3.

Electromagnetic-Thermal Mechanisms and Measurement Boundaries

Gain-temperature analysis requires a clear separation between the electromagnetic quantities that describe radiation and the thermal quantities that describe energy conversion and heat transport. Array gain is controlled by element patterns, spacing, aperture, feed amplitude and phase, losses, mismatch, and mutual coupling; feed-network and aperture changes can alter gain and sidelobes even in the absence of a thermal intervention (Nagy, 2023). Dedicated gain-enhancement structures make the same point: defective-ground and electromagnetic-band-gap modifications can raise measured gain without providing any thermal mechanism, so gain variation cannot be treated as evidence of heating by itself (Rao et al., 2018).

For external exposure, the relevant field may be strongly nonuniform. Measurements of rectangular microstrip radiators in water show that source phase, amplitude, substrate properties, and geometry shape near-field electric-field distributions (Underwood et al., 1992). Numerical field solutions are commonly rooted in discretizations of Maxwell's equations such as the finite-difference time-domain framework, which solves the electromagnetic problem before any thermal interpretation is added (Yee, 1966). Once fields interact with lossy media, frequency-dependent dielectric properties determine absorption; biological-tissue models therefore require dielectric parameters that vary strongly with frequency and composition (Gabriel et al., 1996; Sasaki et al., 2022).

Thermal response is governed by a second layer of physics. Computational dosimetry above 6 GHz distinguishes electromagnetic absorption from the subsequent temperature field because conduction, perfusion, boundary heat transfer, and exposure duration redistribute deposited energy (Hirata et al., 2021). This distinction is fundamental to the present framework: gain describes directional radiation relative to a power reference, whereas temperature reflects local absorption plus heat transport and thermal boundary conditions. Consequently, an apparent gain-temperature association is interpretable only when the thermal object, power reference, and exposure geometry are stated.

Development of Array Architectures and Coupled Validation

Materials and architecture connect the two domains. Graphene illustrates why a high thermal-conductivity material cannot be reduced to a single device-level thermal claim. Suspended monolayer graphene has shown room-temperature thermal conductivity on the order of 4.8-5.3 × 10^3 W m−1 K−1 under the investigated conditions (Balandin et al., 2008), while graphene-filled thermal-interface composites can produce large cross-plane transport improvements that depend on filler loading and interface quality (Shahil & Balandin, 2012). Reviews of graphene heat transport emphasize strong anisotropy and the decisive role of interfaces and substrates (Pop et al., 2012). These properties can influence heat spreading, yet they do not determine antenna gain without the electromagnetic geometry and loss mechanisms.

Array architectures also create electromagnetic trade-offs independent of temperature. Partially reflective surfaces can raise planar-antenna gain through resonant field interaction between the radiator and a superstrate (Feresidis & Vardaxoglou, 2001). Related Fabry-Perot designs use frequency-selective surfaces to broaden or shape high-gain operation (Sheng et al., 2022), while parasitic patches modify current distribution and resonance to increase bandwidth and gain (Kim et al., 2021). Suspended microstrip feed structures can suppress unwanted feed radiation in large radar arrays and thereby improve aperture performance (Anim et al., 2022). Sequential feeding and partially reflective surfaces in a 2 × 2 circularly polarized array similarly show that feed phase and resonant-cavity behavior materially affect gain and bandwidth (Melouki et al., 2022).

Thermal integration becomes especially important when active electronics share the package. Board-level 60 GHz phased-array transmitter modules have been analysed with finite-element and computational-fluid-dynamics models and validated by infrared thermography, demonstrating that chip dissipation, packaging orientation, convection, and heat spreaders can dominate junction temperature even when the antenna aperture is unchanged (Cheng et al., 2013). Temperature-dependent microstrip-array measurements have also been reported using reflection and radar-cross-section approaches, showing that resonance and gain can change as material and geometric properties vary with temperature (Mernyei & Voelgyi, 1990). The theoretical pathway is therefore bidirectional: power loss and electronics dissipation can create heat, and the

resulting material or structural changes can feed back into impedance, efficiency, and gain.

Interpretation Challenges, Competing Explanations, and Unresolved Issues

External-medium heating introduces a third pathway. Area-averaged transmitted power density has been proposed as a predictor of surface temperature elevation, but its relationship depends on frequency and averaging area (Funahashi, Hirata, et al., 2018). Patch-array exposure studies likewise show that four- and nine-element configurations produce localized power-density patterns whose interpretation changes with the averaging convention (Funahashi, Ito, et al., 2018). Anatomical modelling at 28 GHz demonstrates that beam steering and source geometry can change temperature elevation even when nominal source settings are similar (He et al., 2018). Theoretical work on spatial averaging therefore cautions against replacing local exposure fields with a single far-field gain value (Neufeld et al., 2018).

Classical hyperthermia research makes the separation between deposition and heat transfer explicit. Four-antenna microwave arrays produce power and temperature patterns that depend on tissue-equivalent medium and spatial position; phantom and canine measurements showed that the final temperature distribution reflects both deposition and thermal transport (Denman et al., 1988a). Altering antenna spacing and insertion depth shifts where maximum power and temperature occur and can make conductive redistribution dominate the central temperature field (Denman et al., 1988b). Finite-element bioheat calculations for 915 MHz dipole arrays further demonstrate that insertion depth can radically change the volume reaching therapeutic temperature, reinforcing the need for adequate thermometry and treatment planning (Mechling et al., 1992).

Modern multiphysics studies extend these principles. Coupled microwave-heating simulations of water link electromagnetic, thermal, and fluid-flow fields and reveal sensitivity to temperature-dependent material properties and solver assumptions (Vencels et al., 2019). Microwave-sensitive coatings show that irradiation frequency, antenna type, distance, and surface geometry jointly influence heating rate and uniformity (Xiao et al., 2025). Hyperthermia applicators map antenna excitation to power density, specific absorption rate, and temperature rather than treating those quantities as interchangeable (Suseela & Wahid, 2020), and optimization of a four-element arrangement shows that

amplitude and phase control can localize absorbed energy in a target region (Elkayal et al., 2024). Together, these studies define the review's interpretive boundary: temperature may alter radiation, device dissipation may heat the antenna system, or emitted fields may heat an external medium, but each pathway requires different controls and validation.

This framework guides the Results: Theme 1 treats temperature as an input or condition for radiation behaviour; Theme 2 treats internal losses, materials, and integrated electronics as thermal pathways; Theme 3 treats an external object as the thermal receiver; and Theme 4 evaluates whether those relationships transfer to a planar 2 × 4 geometry.

Research Gap, Aim, and Review Questions

Existing reviews of related topics address thermal management at system level, for example heat-dissipation strategies for 5G and 6G base stations (Dbouk & Mourad, 2025), whereas the question of how gain, accepted power, thermal object, and boundary conditions must be defined and validated together in microstrip-array evidence has not, to the authors' knowledge, been mapped systematically. The gap addressed here is therefore methodological as well as empirical: which evidence exists, under which conditions it was obtained, and what is required to test a planar 2 × 4 gain–temperature relationship.

Against this heterogeneous background, the central problem is not whether temperature and antenna gain can appear in the same study, but what physical object is heated, which direction of interaction is tested, how gain and power are defined, and whether electromagnetic and thermal observations are measured or modelled under comparable conditions. This scoping review therefore maps three principal pathways: temperature acting on radiation behaviour; internally generated or electronics-related heat affecting the antenna system; and external electromagnetic exposure producing heating in a separate medium. The Population-Concept-Context logic is adapted to the engineering field: eligible evidence concerns microstrip or patch arrays, substantive electromagnetic-thermal relationships, and communication, radar, space, wireless-power, or deliberate-heating contexts. Four questions guide the review: (1) which mechanisms and directions of gain-temperature interaction are studied; (2) how gain, power, temperature, and boundary conditions are operationalized and validated; (3) which methodological and reporting gaps limit interpretation; and (4) what evidence is directly applicable, conditionally transferable, or insufficient

for a planar 2 × 4 microstrip array. The scientific contribution is a mechanism-based evidence map that distinguishes gain from power deposition, separates thermal compartments, and converts the observed heterogeneity into explicit validation requirements rather than a universal causal claim.

Relevance to transportation and navigation systems. Microstrip arrays form part of navigation, communication, and surveillance subsystems, including satellite-navigation antennas designed for high-temperature operation (F. Xu & Zhang, 2025) and radar and communication arrays whose performance must be maintained under thermal stress (R. Li et al., 2023). Distinguishing whether a thermal change reflects antenna behaviour, electronics dissipation, or external exposure therefore supports the reliability assessment of equipment used in air navigation and other transport communication infrastructure, which is the application context of the authors' field.

The remainder of the article is organized as follows. Section 2 describes the scoping-review methods, the use of AI assistance, and the interim evidence status. Section 3 reports the charted evidence for the four prespecified themes (Sections 3.1–3.4), summarizes the included reports (Table 5), and integrates the findings with their methodological implications and limitations (Section 3.5). Section 4 states the bounded conclusions and priorities for future 2 × 4 validation.

Research Method

Search Strategy

This review was designed as a scoping review because the purpose is to map heterogeneous mechanisms, operational definitions, validation practices, and evidence gaps rather than estimate a single comparative effect (Munn et al., 2018). The protocol follows Population-Concept-Context reasoning and links the questions, eligibility rules, search, selection, charting, and presentation as recommended for scoping reviews (Peters et al., 2020). A detailed protocol was prepared using the Generalized Systematic Review registration structure so that planned search, screening, extraction, synthesis, and descriptive appraisal decisions could be made explicit before the definitive review stages (Peters et al., 2022; van den Akker et al., 2023). The present manuscript reports the evidence state reached from the supplied seed export and full-text batch; it does not claim that the definitive database search, dual-reviewer screening, or OSF registration has been completed.

The reporting structure is aligned with the PRISMA extension for scoping reviews, while search documentation follows PRISMA-S principles (Tricco et al., 2018; Rethlefsen et al., 2021). PRISMA 2020 terminology is used to distinguish records, reports, and underlying studies in the selection accounting (Page et al., 2021). Because the available workflow includes preliminary retrieval rather than a completed multi-database search, the flow diagram is explicitly labelled interim. The review also adopts the principle that charting, descriptive analysis, and presentation should be designed around the review questions and should not be interpreted as a substitute for effect estimation or certainty grading (Pollock et al., 2023).

Search development used Scopus as the principal database and Web of Science Core Collection as the planned supporting database. The principal Scopus query was TITLE-ABS-KEY((microstrip OR "micro-strip" OR patch) AND antenna* AND array* AND (temperatur* OR thermal OR heating OR electrothermal OR thermomechan* OR "heat transfer" OR "heat dissipation" OR cooling OR heatsink* OR "heat sink*")). A gain-focused diagnostic subset added (gain OR directiv* OR "radiation efficiency" OR "power density"), and a geometry-sensitive search targeted "2x4", "2 x 4", "4x2", "4 x 2", "eight element*", and "8 element*" expressions. Equivalent Web of Science Topic searches were prespecified. The intent of multiple query forms was sensitivity rather than additive counting; records from all searches are to be unioned and deduplicated. Structured peer review of electronic strategies is recommended because errors in Boolean logic, syntax, field translation, or limits can materially alter retrieval (McGowan et al., 2016). Citation chasing is also planned as a supplementary identification route for studies connected through references rather than shared terminology (Haddaway, Grainger, & Gray, 2022).

Protocol and supplementary materials. The review protocol was prepared using the Generalized Systematic Review registration structure but has not yet been registered; registration is a planned step before the definitive review. The principal Scopus search string and the additional query forms are reported in full above to support reproducibility (Rethlefsen et al., 2021).

Eligibility Criteria

Eligibility required arrays whose radiating elements are microstrip or patch structures and a substantive operational thermal condition or electromagnetic-thermal analysis linked to radiation, electromagnetic loss, energy deposition, or

integrated array operation. Fabrication-temperature-only reports, use of "low-temperature cofired ceramic" only as a technology label, material-only studies without an operational array link, nonarray antennas, and unrelated radiators were excluded from the primary evidence set. Eligible sources could be analytical, numerical, experimental, or mixed original studies in journal articles, full conference papers, or sufficiently detailed technical reports. Reviews and textbooks were used only for background and citation discovery. Evidence was coded as A-G when gain and an object-specific thermal quantity were linked under documented conditions, A-R when another radiation metric rather than gain was linked to thermal behaviour, and B when the study provided relevant mechanism evidence without a directly paired radiation-thermal response.

Box 1. Population–Concept–Context (PCC) framework adapted to the engineering field.

Element	Definition used for eligibility
Population	Microstrip or patch antenna arrays (planar, conformal, or integrated), including the planar 2 × 4 geometry of interest.
Concept	Substantive electromagnetic-thermal relationships: temperature acting on radiation behaviour, internally generated heat affecting the array system, or electromagnetic exposure heating an external medium; with gain or other radiation metrics, power reference, and thermal quantities charted together.
Context	Communication, radar, space, wireless-power, and deliberate-heating applications; analytical, numerical, experimental, or mixed original studies.

Screening, Selection, Data Charting, and Descriptive Appraisal

Record management followed a DOI-first deduplication sequence, then normalized-title comparison, author-year checks, and manual review of near-matches. Structured duplicate handling is important because formatting differences can otherwise lead the same bibliographic report to be screened repeatedly (Bramer et al., 2016). In the supplied 366-record seed export, no confirmed bibliographic duplicate required deletion. Title and abstract screening classified 60 records as high relevance, 54 as uncertain and requiring clarification, and 252 as not prioritized. Nine full-text reports were subsequently supplied: seven from the high/uncertain pool and two from the earlier non-priority pool. All nine underwent full-text assessment; five were provisionally eligible and four were excluded for wrong radiating architecture or absence of a substantive operational array-thermal link. The remaining 107 high/uncertain records had not been supplied as full texts and are therefore pending retrieval, not scientific exclusions.

Data charting retained report identifiers, DOI, geometry, frequency, substrate and metallization, feed and excitation, gain or radiation metric, power reference, thermal object, baseline and range, heat source or exposure, boundary

conditions, numerical or experimental method, calibration, controls, uncertainty, relationship direction, and source page or figure. Extraction recommendations for scoping reviews emphasize that charting variables should answer the review questions and remain traceable to the underlying reports (Pollock et al., 2023). Numerical values were not imputed. Missing information was marked not reported or unclear, and source contradictions were preserved rather than silently reconciled. Descriptive appraisal covered five domains: power and comparability, electromagnetic validation, thermal validation, numerical credibility, and attribution/reporting. This review-specific framework was used to characterize interpretability; it was not converted into an overall quality score or used as an exclusion threshold.

Operational definitions of the appraisal domains. D1 (power and comparability) concerned whether accepted radiofrequency power, duty cycle, and operating conditions were stated and matched between thermal states. D2 (electromagnetic validation) concerned whether gain or other radiation metrics were measured or validated, including gain-reference calibration. D3 (thermal validation) concerned whether the thermal object, thermometry method, calibration, stabilization, emissivity, repeatability, and uncertainty were documented. D4 (numerical credibility) concerned whether mesh convergence, boundary-condition sensitivity, energy balance, and independent physical validation were reported. D5 (attribution and reporting) concerned whether results were attributed to the correct object and condition and whether values were consistent across the abstract, text, tables, and figures. The coding categories are defined under Table 4.

Figure 1 presents the interim selection flow. The figure was generated from the screening workbook and the full-text extraction log, and its construction follows the logic of PRISMA flow diagrams (Haddaway, Page, et al., 2022). At this stage, the 107 pending reports prevent the flow from being interpreted as a completed review search. Screening and extraction were AI-assisted and await independent human confirmation. Final protocol amendments, definitive search logs, dual-reviewer decisions, and a completed flow diagram should be versioned rather than overwriting the current audit trail, consistent with the transparency goals of prospective registration (van den Akker et al., 2023).

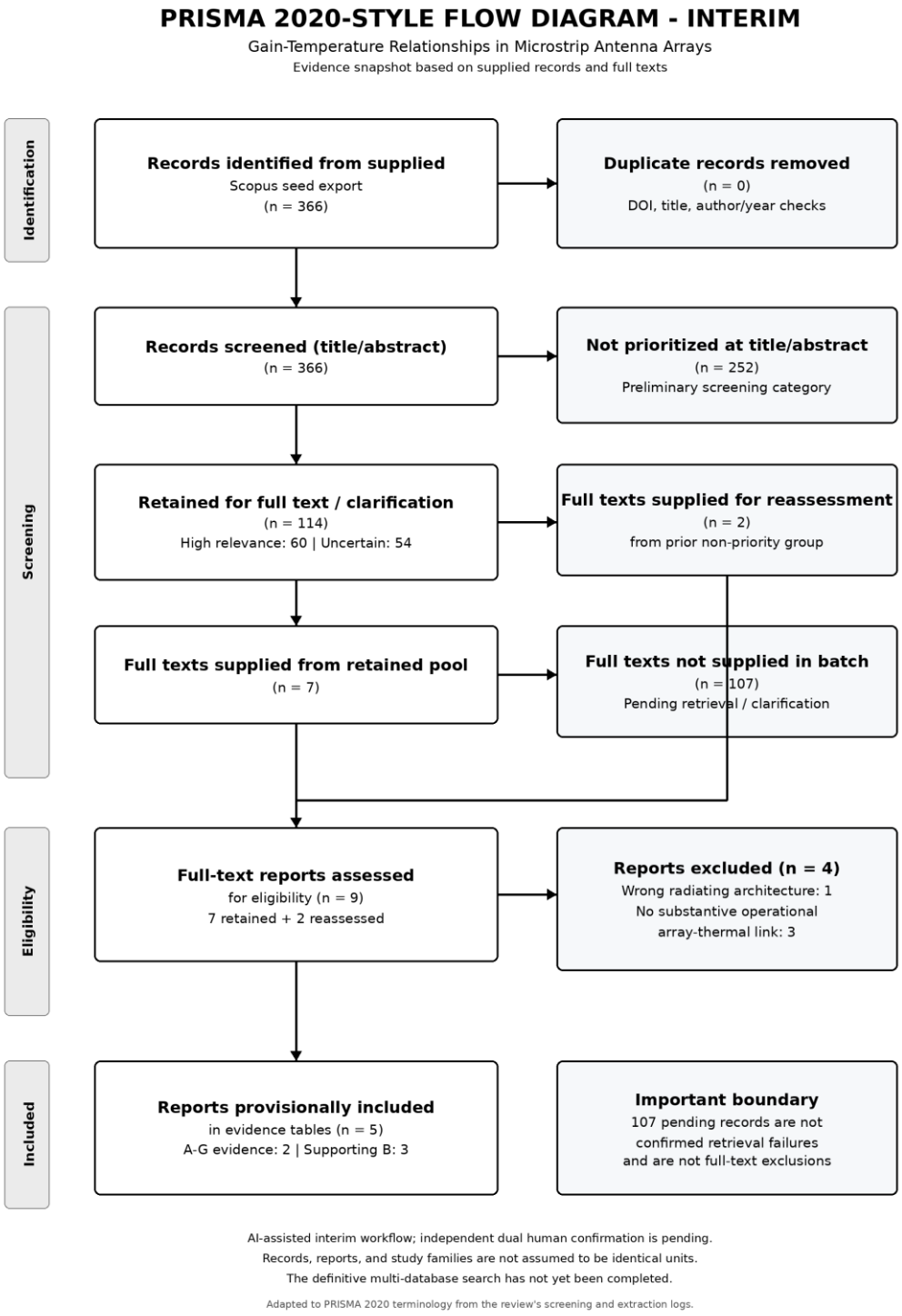


Figure 1. Interim PRISMA 2020-style flow diagram for the supplied seed export and full-text batch. The 107 pending records are not confirmed retrieval failures and are not full-text exclusions. Counts are interim and will be updated when the pending records are retrieved and the definitive search is completed.

2.4 Use of AI Assistance and Reviewer Confirmation

Screening and data extraction were AI-assisted. AI-generated classifications are treated as provisional decisions that do not enter the evidence map as final until they are confirmed by human reviewers, and no AI-assisted decision was used to impute missing values.

Planned confirmation. Before the review is finalised, title/abstract and full-text decisions and all extracted data are to be verified independently by two human reviewers, disagreements are to be resolved by discussion or by a third reviewer, and the level of agreement is to be reported. At the time of writing this step has not been completed, which is why the review is reported as interim.

Selection of the full-text batch. Seven of the nine full texts came from the high/uncertain pool and two from the earlier non-priority pool. All nine were assessed against the same prespecified criteria, so the origin of a report did not alter the eligibility rules applied.

Results and Discussion

Section 3 reports the charted evidence for the four prespecified themes (Sections 3.1–3.4), with interpretation limited to what each report supports; Section 3.5 integrates the findings and states their methodological implications and limitations. Table 5 summarizes the five provisionally eligible reports by theme and evidence code.

Temperature-Dependent Gain and Radiation Characteristics (Theme 1)

Two reports populated the temperature-dependent radiation theme (Table 1). The clearest array-level thermal intervention was the conformal 4 × 4 ceramic array reported by P. Li and colleagues. The study modelled room-temperature and 600 °C conditions and also exposed antenna-layer samples to 600 °C for approximately 20 minutes. The experimental procedure then removed the samples near 200 °C and allowed them to cool before radiofrequency assessment. The measured peak gain at 13 GHz changed from 22.07 to 20.46 dBi, giving a peak-to-peak difference of 1.61 dB at that operating point. The source also reports a maximum measured reduction of "2.91 dBi"; the review retained that printed value and did not reinterpret it as a universal temperature coefficient. Because the radiofrequency measurement followed cooling, the experiment supports retained performance after high-temperature exposure, whereas in-situ hot-state gain remains numerical (P. Li et al., 2026).

The second report used a planar 2 × 2 circularly polarized array at 28 GHz. The fabricated array was measured in a radiofrequency chamber, while printed insulation and daisy-chain specimens underwent 200 thermal cycles from −60 to 140 °C. The main text reports a measured gain of 6.44 dB and an 8.00 GHz impedance bandwidth, whereas the abstract reports 6.33 dB and 6.8 GHz. The review preserved both source accounts rather than averaging them. Coupon resistance changed from a reported mean of 0.92 to 0.96 Ω, but no before-and-after thermal-cycle gain curve was supplied for the same array. The evidence therefore supports process and interconnect qualification, not a directly measured gain-temperature function (Yoo et al., 2025).

Across these reports, the strongest distinction was not the magnitude of gain change but the timing and object of measurement. A hot-state simulation, a post-cooling prototype test, and a thermally cycled coupon answer different questions. Neither report provided a calibrated, repeated, in-situ gain measurement across a controlled temperature sequence for the complete planar array. The table therefore classifies the ceramic conformal study as A-G evidence with an important post-exposure boundary and the printed satellite array as supporting B evidence.

Table 1. Temperature-dependent gain and radiation characteristics of provisionally included microstrip antenna-array reports.

References	Array / frequency	Temperature exposure	Gain / radiation metrics	Methods / controls	Relationship / validity
Li et al. (2026) P02 / R229 Publisher / DOI	Conformal 4 × 4 alumina array; 300 mm curvature radius; Ku band. Printed silver conductors and a 1-to-16 feed. [pp. 5–6, 13]	Model: room-temperature versus 600 °C material/structural conditions. Experiment: furnace hold at 600 °C for approximately 20 min; removed near 200 °C and cooled to room temperature before RF assessment. [pp. 5–9, 13]	Measured before / after treatment: peak gain 22.07 / 20.46 dBi at 13 GHz; −10 dB bands 12.01–15.8 / 11.63–15.71 GHz. Modelled hot gain loss up to 3 dB. Author-reported maximum measured reduction: “2.91 dBi” (source unit). [pp. 9–11, 13]	Before/after prototype comparison, furnace images, gain and pattern curves. Alumina permittivity/loss characterized for hot-condition modelling. RF source power, gain-reference calibration, repeat count and temperature at RF measurement are not fully reported. [pp. 5, 10–11, 13]	A-G; M1. Supports numerical hot-state performance and measured performance after thermal exposure, not measured in-situ gain at 600 °C. Peak-to-peak difference at 13 GHz = 1.61 dB, calculated from reported gains; not a universal temperature coefficient. [pp. 10–11, 13]
Yoo et al. (2025) P05 / R050 Publisher / DOI	Planar 2 × 2 circularly polarized array; 28 GHz; 20 × 24 × 1.56 mm. Acrylate dielectric and printed silver. Sequential-rotation feed. [pp. 2–4, 7–8]	Printed insulation and daisy-chain coupons, not a paired RF-tested array, underwent 200 cycles from −60 to 140 °C. Chamber: TCC-150. [pp. 6–7, Fig. 8]	Array body/conclusion: measured gain 6.44 dB at 28 GHz, impedance bandwidth 8.00 GHz; modelled gain 9.31 dB. Abstract instead gives peak gain 6.33 dB and	Coupon mean resistance: 0.92 → 0.96 Ω; reported increase 4.35%. RF chamber measurements are described separately. No before/after thermal-cycle gain	B; M1-related qualification support only. Electrical continuity of printed coupons does not establish temperature-stable array gain. Conflicting gain/bandwidth and coupon-dispersion

References	Array / frequency	Temperature exposure	Gain / radiation metrics	Methods / controls	Relationship / validity
			bandwidth 6.8 GHz. Units retained. [pp. 1, 4, 8, 10]	curve of the array is supplied. [pp. 6–9]	statements are retained in the discrepancy log. [pp. 1, 7–10]

Internal Heating, Materials, and Thermal Management (Theme 2)

Three reports informed internal thermal mechanisms, material pathways, and thermal management (Table 2). A 2 × 2 patch array on a modified bismaleimide-triazine composite was accompanied by material thermal tests, a separate light-emitting-diode heat-spreading demonstration, and a chip thermal model. The composite formulation was reported with relative permittivity 3.25 and loss tangent 0.0028 at 10 GHz. Thermal conductivity was reported as 0.613 W m−1 K−1 compared with 0.165 W m−1 K−1 for the comparison material, while a chip model predicted 77 versus 91 °C. The array itself had measured reflection data and a simulated gain of 11.01 dBi at 10.55 GHz, but no array thermometry or measured gain-temperature sweep. The study was therefore retained as material-level support, and the review did not reassign the 12 W light-emitting-diode or 5 W chip loads to the antenna (H. Wang et al., 2026).

A second material study characterized LiGaSiO4 and related ceramics before demonstrating a simulated 4 × 8, 36 GHz patch array. For the LiGaSiO4 substrate used in the array example, thermal conductivity was reported as 8.4 W m−1 K−1, coefficient of thermal expansion as 7.5 ppm °C−1 over 25-500 °C, and temperature coefficient of resonant frequency as −63 ppm °C−1. The simulated array reached 18.3 dBi peak realized gain and 93.3% peak efficiency. Because the thermal properties were measured on material specimens and the antenna remained a nominal-state simulation, this report was coded as supporting mechanism evidence rather than a coupled array experiment (W. Wang et al., 2025).

ETC-Net provided the most direct numerical bridge between array electromagnetic and thermal fields. The numerical corpus covered square patch arrays from 2 × 2 to 5 × 5, with 10 W per port, an initial temperature of 293.15 K, a convection coefficient of 3 W m−2 K−1, and a substrate thermal conductivity of 0.3 W m−1 K−1. Reported COMSOL gains increased with array size and were closely reproduced by the learned network, while surface-temperature maps were also predicted. However, the displayed gain examples and thermal examples used different frequencies, and the paper did not tabulate paired maxima from identical cases. The review therefore treated the work as numerical

electromagnetic-thermal co-prediction, not as evidence of measured feedback or a gain-temperature slope (Jia et al., 2025).

The descriptive appraisal reinforced these distinctions. Power and comparability were adequately described for the ETC-Net modelling cases but remained unclear for several experiments because accepted radiofrequency power, duty cycle, or matched operating conditions were not reported. Electromagnetic validation ranged from measured reflection coefficients to modelled gain, while direct gain calibration under thermal conditions was generally absent. Thermal validation was strongest where the thermal object and procedure were explicitly identified, yet calibration, stabilization, emissivity, repeatability, and uncertainty were incompletely reported. Numerical credibility was not rejected, but mesh convergence, boundary sensitivity, energy balance, and independent physical validation were often unclear. These are domain-level interpretive concerns rather than exclusionary scores.

Source-level inconsistencies were retained as part of the evidence map because resolving them without author clarification would create unreported reviewer corrections. In the bismaleimide-triazine paper, the Methods and Results use different directional descriptions for thermal transport, and the reported increase from 0.165 to 0.613 W m−1 K−1 is labelled as 282%, whereas the raw values imply a different percentage; the review therefore charts the raw values and flags the inconsistency (H. Wang et al., 2026). In the printed satellite-array paper, the abstract and main text differ in both gain and bandwidth, and the prose and table give different post-cycle dispersion values; all accounts remain visible (Yoo et al., 2025). In ETC-Net, the manuscript reports 6,188 numerical cases but the data-availability statement says no data were used, and the displayed gain and thermal examples are not identical operating cases (Jia et al., 2025). These discrepancies do not automatically invalidate the studies, but they reduce the precision with which a quantitative cross-study relationship can be reconstructed. The appraisal therefore separates "concern identified" from "unclear/not reported" and avoids a summed quality score.

Table 2. Internal thermal mechanisms, material pathways, and management evidence linked to array performance.

References	Array / material	Heat source / control	Power / thermal setting	Radiation / thermal outcomes	Validation / limitations
Wang, H., et al. (2026) P01 / R339 Publisher / DOI	Fabricated planar 2 × 2 patch array on 75 wt% amino-	Material heat spreading and thermal-interface	Coupon: 60 °C plate. Separate LED: 12 W; chip	Simulated array gain 11.01 dBi at 10.55 GHz and peak	B; material-level M1/M2 support. Actual array impedance is measured,

References	Array / material	Heat source / control	Power / thermal setting	Radiation / thermal outcomes	Validation / limitations
	functionalized SiO2 / modified bismaleimide–triazine composite. [pp. 8–9, Fig. 6]	function. Tests use a heated coupon, a separate LED/heat-sink assembly, and a chip model; none is an operating-array thermal test. [pp. 6–7]	model: 5 W. Dielectric-temperature test: −40 to 150 °C at 10 GHz. CTE averaged over 50–250 °C. Array RF power NR. [pp. 6–8]	efficiency 84%; measured S11 is reported separately. Material conductivity 0.613 versus 0.165 W/(m·K). Chip model: 77 versus 91 °C. CTE 18.7 ppm/°C. [pp. 6–9]	but no array thermometry or measured gain–temperature link. Thermal-transport direction and percentage statements are inconsistent; preserve raw values. [pp. 2, 6–9]
Wang, W., et al. (2025) P03 / R303 Publisher / DOI	Simulated 4 × 8 planar array on LiGaSiO4 (LGS), approximately εr = 5.2; 36 GHz. Other tested ceramics are not interchangeable with the LGS antenna substrate. [pp. 2–3, 7–8]	Measured thermal conductivity, expansion and resonant-frequency temperature coefficient of ceramics; proposed heat-management benefit. No operating-array heat-source test. [pp. 3–5, 8]	LGS conductivity 8.4 W/(m·K); thermal measurements discussed at 30 °C. CTE 7.5 ppm/°C over 25–500 °C. LGS TCF −63 ppm/°C; its temperature interval is not specified in this PDF. Array RF power NR. [pp. 3–4, 8]	HFSS array: peak realized gain 18.3 dBi; peak efficiency 93.3%; −10 dB band 35.38–36.55 GHz. No measured array temperature, temperature rise or gain change. [pp. 7–8, Fig. 4]	B; material-level M1/M2 support. Thermal material tests and a nominal-state EM design are separate evidence. Several characterization methods refer to another paper not supplied; no independent array validation. [pp. 2, 7–8]
Jia et al. (2025) P06 / R166 Publisher / DOI	Numerical rectangular-patch arrays: 2 × 2, 3 × 3, 4 × 4 and 5 × 5; 1.45–1.85 GHz. Common substrate 600 × 600 × 1.5 mm. [p. 7]	One-way field/loss-to-temperature modelling in COMSOL and a learned surrogate. Thermal field is on the upper array surface; no ambient-air or external-medium heating experiment. [pp. 3–7, 11]	10 W per port; initial temperature 293.15 K; convection coefficient 3 W/(m²·K); substrate conductivity 0.3 W/(m·K). This is not fixed total-array power. [p. 7]	COMSOL / network gains: 8.29/8.17, 11.27/11.05, 14.57/14.33, 17.17/16.91 dBi (ascending sizes). Temperature maps are reported, but maxima are not tabulated. Gain examples and thermal-map examples use different frequencies. [pp. 9–11, Table 5; Fig. 11]	A-G numerical co-prediction; M2, not demonstrated feedback M4. 6,188 simulated cases are training data, not independent studies. No physical thermometry or heated-prototype RF validation. No paired numerical slope is inferred from the displayed gain and thermal examples. [pp. 7–13]

External-Medium Heating (Theme 3)

No report among the nine full texts assessed was eligible for this theme, so no evidence table could be populated. The external-medium studies discussed in Section 1 (for example, work on hyperthermia arrays and millimetre-wave exposure) serve as contextual literature and do not enter the eligibility accounting. This theme therefore remains unpopulated in the supplied corpus; whether eligible studies exist among the 107 pending high/uncertain records cannot yet be stated.

Array Geometry, 2 × 4 Configurations, and Evidence Gaps (Theme 4)

Table 4 cross-maps the five eligible reports against geometry and applicability to a planar 2 × 4 array. None directly tested that geometry. The modified bismaleimide-triazine study used a planar 2 × 2 array; doubling the number of

elements would alter feed loss, accepted power, aperture, and thermal boundaries, so its material results are only conditionally transferable (H. Wang et al., 2026). The ceramic high-temperature study used a conformal 4 × 4 array with a 300 mm curvature radius and a 1-to-16 feed. Its thermal-exposure procedure is informative for protocol design, but its numerical gain reduction cannot be transferred directly to a planar eight-element array (P. Li et al., 2026).

The LiGaSiO4 study used a 4 × 8 simulated array at 36 GHz, while the printed satellite study used an actual 2 × 2 array at 28 GHz. Both provide useful information about substrate or fabrication qualification, yet neither establishes how an eight-element 2 × 4 aperture would redistribute current, feed losses, accepted power, or temperature (W. Wang et al., 2025; Yoo et al., 2025). ETC-Net included 2 × 2, 3 × 3, 4 × 4, and 5 × 5 square arrays, but not a rectangular 2 × 4 case. Because the nominal source power was 10 W per port, total source power increased with element count; the array-size trend therefore cannot be interpreted as a fixed-total-power experiment isolating the thermal consequence of gain (Jia et al., 2025).

Four observations follow from the cross-theme map. First, measured in-situ hot gain was absent from the five eligible reports. Second, no full-text study in the supplied set validated a planar 2 × 4 gain-temperature relationship. Third, the external-medium heating table remained empty. Fourth, no experiment held total power and the relevant exposure geometry fixed while changing array gain alone. These absences define the principal evidence gaps within the supplied corpus. They do not justify relaxing eligibility to reach a target number of studies, and they do not establish that the corresponding phenomena are physically impossible.

Table 3. Geometry-specific evidence and applicability to planar 2 × 4 microstrip antenna arrays.

References	Verified geometry	Operating / feed settings	Gain–thermal linkage	Validation / controls	2 × 4 applicability / gaps
Wang, H., et al. (2026) P01 / R339 Publisher / DOI	Planar 2 × 2 radiating patch array; schematic and fabricated specimen in Fig. 6. [p. 9]	10.55 GHz nominal; printed corporate feed; composite εr 3.25 and loss tangent 0.0028 at 10 GHz. [pp. 7–9]	B: material thermal transport and dielectric-temperature behavior plus nominal EM array performance; no paired array G(T). [pp. 6–9]	Measured S11; modelled gain/efficiency. Thermal coupons, LED test and chip simulation are separate. [pp. 6–9]	Supports candidate-material selection only. Doubling the number of radiators to 2 × 4 is not tested; feed loss, accepted power, geometry and thermal boundaries would change.
Li et al. (2026) P02 / R229 Publisher / DOI	Conformal 4 × 4; curvature radius 300 mm, 16 radiators. Not a planar eight-	Ku band; 1-to-16 power division and phase compensation; 0.88λ feed spacing as	A-G: hot-state simulation and before/after furnace-exposure RF measurement. Post-	Material characterization, numerical mechanics/EM analysis, prototype	Transferable approach to reporting thermal exposure, not transferable numerical gain loss.

References	Verified geometry	Operating / feed settings	Gain–thermal linkage	Validation / controls	2 × 4 applicability / gaps
	element layout. [pp. 6, 10, 13]	reported. Alumina layers and printed silver. [pp. 5–6]	cooling evidence must stay distinct from hot-operation evidence. [pp. 9–13]	and furnace procedure. No controlled planar 2 × 4 comparison. [pp. 5–13]	Curvature, element count and feed differ.
Wang, W., et al. (2025) P03 / R303 Publisher / DOI	Planar 4 × 8; 32 patches on 34 × 22 mm substrate; configuration shown in Fig. 4b. [p. 7]	36 GHz; Chebyshev amplitude synthesis; array feed 50 Ω. Design and validation are numerical. [pp. 2–3, 7–8]	B: measured LGS properties, including conductivity/CTE/TCF, plus a nominal-state array simulation. [pp. 3–5, 8]	No fabricated array RF result, array temperature measurement or coupled thermal sweep. [pp. 7–8]	Material/design context only. A 4 × 8 array or its unspecified subarray is not evidence for a planar 2 × 4 configuration.
Yoo et al. (2025) P05 / R050 Publisher / DOI	Planar 2 × 2; actual printed four-element specimen. [pp. 4, 8, Figs. 5 and 10]	28 GHz; 6.65 mm element spacing; 90° sequential phase progression. Total footprint 20 × 24 × 1.56 mm. [pp. 3–4, 7–8]	B: material/interconnect qualification; no paired temperature-dependent array gain measurements. [pp. 6–9]	Nominal RF prototype measured separately from thermally cycled coupons. No 2 × 4 model or prototype. [pp. 6–9]	Printing and coupon-validation methods may inform a design study; neither gain nor thermal-cycle survival can be assigned to an untested 2 × 4 array.
Jia et al. (2025) P06 / R166 Publisher / DOI	Planar square arrays 2 × 2 to 5 × 5; equal 108 mm spacing. The PIFA extension is a separate radiator example within the same report, not another study. [pp. 7, 9, 13]	1.45–1.85 GHz; 10 W per port. Nominal summed source powers are 40, 90, 160 and 250 W, calculated as element count × 10 W; accepted power NR. [p. 7]	A-G, numerical M2: gain and thermal fields from one simulation/surrogate framework; no demonstrated temperature-to-EM feedback. [pp. 3–7, 11]	COMSOL-labelled training/test samples; geometry-held-out validation and physical measurements not established. Displayed gain and thermal examples are not identical cases. [pp. 7–11]	No rectangular 2 × 4 test case. Performance on square arrays does not verify generalization to rectangular arrays, fixed-total-power gain changes or environmental-air heating.

Table 4. Descriptive engineering appraisal of the five provisionally included reports.

References	D1	D2	D3	D4	D5	Evidence role
Wang, H., et al. (2026) P01 / R339 Publisher / DOI	U	U	C	U	C	B — material support
Li et al. (2026) P02 / R229 Publisher / DOI	U	U	U	U	C	A-G — modelled hot / measured post-exposure
Wang, W., et al. (2025) P03 / R303 Publisher / DOI	U	U	U	U	D	B — material support
Yoo et al. (2025) P05 / R050 Publisher / DOI	U	U	U	U	C	B — coupon qualification
Jia et al. (2025) P06 / R166 Publisher / DOI	D	D	U	U	C	A-G — numerical co-prediction

Appraisal codes: D = adequately described; C = concern identified; U = unclear/not reported; NA = not applicable. The framework is descriptive and review-specific; no overall score or exclusion threshold was applied.

Table 5. Summary of the five provisionally eligible reports by theme, evidence code, and applicability to a planar 2 × 4 array.

Report	Theme	Array	Evidence code	Measured vs modelled	Direct 2 × 4 evidence
Li et al. (2026)	1	Conformal 4 × 4 alumina array, Ku band	A-G	Hot state modelled; RF measured after exposure and cooling	No

Yoo et al. (2025)	1	Planar 2 × 2 circularly polarized array, 28 GHz	B	RF prototype measured; thermal cycling on coupons only	No
H. Wang et al. (2026)	2	Planar 2 × 2 patch array on modified bismaleimide-triazine composite, 10.55 GHz	B	Material thermal tests; gain simulated, reflection measured	No
W. Wang et al. (2025)	2	Simulated 4 × 8 planar array, 36 GHz	B	Material properties measured; array simulated only	No
Jia et al. (2025)	2	Square patch arrays, 2 × 2 to 5 × 5 (numerical)	A-G (numerical co-prediction)	Modelled only; no measured feedback	No (no rectangular 2 × 4 case)
None	3	No eligible report	—	—	—

Integrated Discussion and Implications

Studies in this section other than the five provisionally eligible reports are contextual literature (see Section 1.1) and are not counted as evidence in the eligibility accounting.

The mapped evidence supports a mechanism-first interpretation rather than a single gain-temperature law. Application studies show that geometry, integration level, and thermal object vary widely: conformal rocket arrays report gain alongside an operational temperature context (Pascawati et al., 2024), while 60 GHz antenna-in-package work separates electromagnetic measurements from thermal simulations of the package (H. Xia et al., 2023). Thermal-vacuum qualification of a 6 × 6 circularly polarized array is likewise reported separately from scan-dependent gain (Kang et al., 2026), whereas a high-temperature navigation array reports radiation performance across a specified thermal interval (Y. Liu et al., 2017). These examples reinforce the review finding that "temperature" may be an environmental condition, a qualification load, a simulated package temperature, or an actively measured state; treating them as one variable would obscure the actual evidence pathway.

The same discipline is necessary for exposure studies. Numerical 28 GHz human-exposure work maps absorbed electromagnetic energy in anatomical models but does not automatically provide measured ambient heating (Morelli et al., 2021). Multiport smartphone-antenna studies combine communication and exposure metrics, yet mean effective gain, efficiency, and exposure quantities remain conceptually distinct (Kour et al., 2023). A 24.9 GHz 1 × 4 microstrip array with metasurface loading is especially informative because electromagnetic and thermal simulations are reported together over several input powers, with a maximum modelled scalp temperature rise of 0.43 °C at the highest condition;

nevertheless, changing input power is not an isolated gain intervention (Du et al., 2025). Thermal-wave imaging of the field around a 2 × 2 patch array further shows that an absorbing screen can convert local field distribution into a thermal image, making the screen and modulation method part of the measurement chain (Muzaffar et al., 2019).

Internal thermal management provides another non-equivalent route to lower temperature. A modular heat-sink antenna array jointly addresses radiation and cooling in four- and eight-element configurations, but the thermal benefit arises from an integrated heat-transfer architecture rather than from increased gain alone (Celik et al., 2025). A 5.8 GHz 2 × 2 stacked-patch array for wireless power transmission reports measured circularly polarized gain while its thermal analysis compares feed-network substrates, so the electromagnetic and thermal outcomes refer to related but not identical test objects (Lee et al., 2018). Temperature-sensitive liquid-crystal reflectarrays demonstrate that temperature can change both far-field behaviour and switching time (Bildik et al., 2012). Additively manufactured active arrays and integrated amplifier packages similarly show that thermal-management features can reduce electronics temperature while the antenna system maintains its radiofrequency function (Patel et al., 2026). Crossed-dipole base-station arrays with metal heat-removal structures reinforce the same separation between measured radiation and modelled temperature fields (Y. Xu et al., 2023).

The external medium adds biological or material heat-transfer processes that can reverse simple intuition based on power density alone. Age-dependent tissue modelling at 26 and 60 GHz predicts changes in temperature rise even when peak absorption metrics move differently, because tissue properties and geometry influence both deposition and heat flow (Sacco et al., 2021). Infrared measurements of handset-related skin warming have separated insulation and direct-current heating from radiofrequency exposure, demonstrating the need for sham conditions and equipment-heating controls (Straume et al., 2005). More generally, heat-removal strategies can alter radiative and convective transfer: surface treatments may increase emissivity while changing diffusivity (Park et al., 2021), and passive heat-sink optimization balances fin area against restrictions on natural convection (Kirinčić et al., 2025). These thermal mechanisms are outside antenna gain itself but can dominate the observed temperature of the surrounding structure.

The increasing use of data-driven multiphysics models creates both opportunity and a validation challenge. Physics-informed neural networks show how governing equations can constrain learning for forward and inverse problems (Raissi et al., 2019), while broader physics-informed machine-learning frameworks emphasize the need to incorporate physical knowledge without assuming that the learned representation generalizes beyond its training domain (Karniadakis et al., 2021). Reduced-order modelling studies similarly show that combining residual physics and high-fidelity snapshot information can improve predictions for nonlinear systems (Chen et al., 2021). In the present review, these ideas help interpret ETC-Net: agreement with numerical reference data is evidence of surrogate fidelity within the evaluated domain, not experimental confirmation of a causal gain-temperature feedback or proof of transfer to a rectangular 2 × 4 geometry (Jia et al., 2025).

The five provisionally included reports also reveal why source-level provenance must remain explicit. The ceramic conformal-array experiment measures radiofrequency behaviour after a high-temperature exposure and cooling sequence, whereas its hot-state behaviour is numerical; these comparisons answer different questions and should not be merged into one measured temperature coefficient (P. Li et al., 2026). The printed satellite-array paper contains different gain and bandwidth summaries between the abstract and main text, while thermal qualification applies to specimens rather than a paired array gain test (Yoo et al., 2025). The bismaleimide-triazine study reports a thermal-conductivity change whose directional description and percentage are internally inconsistent, so the raw values are safer than an unverified corrected interpretation (H. Wang et al., 2026). The LiMSiO4 work provides measured ceramic properties and a simulated 4 × 8 array, not an experimental gain-versus-temperature sweep (W. Wang et al., 2025). Together, these cases show that reporting quality and experimental design are separate dimensions: missing or inconsistent reporting can limit inference even when the underlying engineering concept remains plausible.

For a future planar 2 × 4 experiment, the most important implication is not to maximize gain first and measure temperature second, but to create matched electromagnetic-thermal comparisons. Geometry, frequency, substrate, feed amplitude and phase, accepted power, duty cycle, distance, orientation, cooling boundaries, and temperature location should be controlled or explicitly varied.

Gain should be measured at the same thermal state whenever the research question concerns temperature-to-radiation feedback; conversely, external heating should be related to local field or absorbed-power metrics rather than inferred from far-field gain alone. The present review also indicates that a 2 × 4 label cannot be treated as transferable by element count: conformal 8 × 1 or 4 × 2 arrangements, active packages, and subarrays can have different aperture axes, feed loss, scan state, and thermal pathways. These recommendations are bounded by an important review limitation: only nine full texts were supplied for formal assessment, five were provisionally included, 107 high/uncertain records remain pending retrieval, and independent dual-reviewer confirmation has not yet been completed. Accordingly, the evidence map is useful for designing a rigorous validation study, but it is not a final estimate of prevalence, effect magnitude, or causality.

Limitations. This review has the following limitations: (i) only Scopus was searched, and the supporting Web of Science search and citation chasing are not yet completed; (ii) 107 high/uncertain records have not been retrieved or assessed; (iii) screening and extraction were AI-assisted and have not yet been confirmed independently by two human reviewers; (iv) the protocol has not been registered; and (v) the descriptive appraisal is review-specific rather than a validated quality instrument. The conclusions are therefore limited to the nine full texts assessed and may change when the definitive search is completed.

Conclusion

This scoping review mapped gain-temperature relationships in microstrip antenna arrays through three distinct pathways: temperature acting on radiation performance, internally generated or electronics-related heat affecting the antenna system, and electromagnetic exposure heating an external medium. The supplied full-text evidence was sparse and heterogeneous. Five of nine assessed reports were provisionally eligible, with only two providing gain-thermal evidence at the array level and three providing supporting material or qualification evidence. No supplied report directly validated a planar 2 × 4 gain-temperature relationship, no eligible full-text report populated the external-medium heating table, and no study isolated the thermal consequence of gain while holding the relevant power and exposure conditions constant. This statement applies only to the nine full texts assessed and should not be read as a claim that such studies do not exist in the wider literature.

The principal methodological finding is that gain, power, temperature, and thermal compartment must be defined together. Hot-state simulation, post-exposure radiofrequency testing, thermally cycled material coupons, package cooling, and exposed-medium thermometry are not interchangeable evidence. For a planar 2 × 4 array, the strongest next step is therefore a paired electromagnetic-thermal experiment with verified geometry, fixed or explicitly controlled accepted power, calibrated gain measurement at the same thermal state, object-specific thermometry, documented boundary conditions, and uncertainty analysis.

The review contributes a mechanism-based framework for separating electromagnetic redistribution from energy deposition and heat transfer. Its conclusions remain bounded by the interim evidence base: the definitive search and retrieval process is incomplete and independent dual-reviewer confirmation remains outstanding. Accordingly, the review identifies validation priorities and evidence gaps rather than a universal causal claim that increasing antenna gain raises environmental temperature. Its main contribution is therefore a framework and a set of validation requirements for a planar 2 × 4 gain–temperature experiment, rather than a conclusion about the absence of evidence.

Acknowledgements

The author expresses gratitude to the agencies, companies, and institutions that have offered support in conducting research and/or writing publications

AI Declaration

The author acknowledges the use of artificial intelligence (AI) tools in supporting the preparation of this manuscript. The author remains fully responsible for the accuracy, originality, and integrity of the research and its findings.

Disclosure statement

No potential conflict of interest was reported by the author(s).

Funding

No funding was received for this work.

References

Anim, K., Danuor, P., Park, S.-O., & Jung, Y.-B. (2022). High-efficiency broadband planar array antenna with suspended microstrip slab for X-band SAR onboard small satellites. Sensors, 22(1), Article 252. https://doi.org/10.3390/s22010252

Balandin, A. A., Ghosh, S., Bao, W., Calizo, I., Teweldebrhan, D., Miao, F., & Lau, C. N. (2008). Superior thermal conductivity of single-layer graphene. Nano Letters, 8(3), 902–907. https://doi.org/10.1021/nl0731872

Banerjee, R., Sharma, S. K., Chieh, J.-C. S., & Farkouh, R. (2022). Investigations of heat sink property of a novel dual linear polarized low cross-polarization X-band phased array antenna employing silicon RFICs-based beamforming network. IEEE Open Journal of Antennas and Propagation, 3, 523–537. https://doi.org/10.1109/OJAP.2022.3170791

Bildik, S., Hamza Karabey, O., Fritzsch, C., & Jakoby, R. (2012). Temperature investigations of liquid crystal based reconfigurable reflectarrays. 2012 15th International Symposium on Antenna Technology and Applied Electromagnetics, ANTEM 2012, Article 6262353. IEEE. https://doi.org/10.1109/ANTEM.2012.6262353

Bramer, W. M., Giustini, D., de Jonge, G. B., Holland, L., & Bekhuis, T. (2016). De-duplication of database search results for systematic reviews in EndNote. Journal of the Medical Library Association, 104(3), 240–243. https://doi.org/10.5195/jmla.2016.24

Celik, F. T., Yarovoy, A., & Aslan, Y. (2025). A novel modular heatsink antenna array with beam scanning and cooling benefits. 2025 19th European Conference on Antennas and Propagation (EuCAP). IEEE. https://doi.org/10.23919/EuCAP63536.2025.10999420

Chen, W., Wang, Q., Hesthaven, J. S., & Zhang, C. (2021). Physics-informed machine learning for reduced-order modeling of nonlinear problems. Journal of Computational Physics, 446, Article 110666. https://doi.org/10.1016/j.jcp.2021.110666

Cheng, H.-C., Ciou, W.-R., Chen, W.-H., Kuo, J.-L., Lu, H.-C., & Wu, R.-B. (2013). Heat dissipation analysis and design of a board-level phased-array transmitter module for 60-GHz communication. Applied Thermal Engineering, 53(1), 78-88. https://doi.org/10.1016/j.applthermaleng.2013.01.006

Dbouk, T., & Mourad, O. (2025). A review on thermal management and heat dissipation strategies for 5G and 6G base stations: Challenges and solutions. Energies, 18(6), Article 1355. https://doi.org/10.3390/en18061355

Denman, D. L., Elson, H. R., Lewis, G. C., Breneman, J. C., Clausen, C. L., Dine, J., & Aron, B. S. (1988a). The distribution of power and heat produced by interstitial microwave antenna arrays: I. Comparative phantom and canine studies. International Journal of Radiation Oncology, Biology, Physics, 14(1), 127-137. https://doi.org/10.1016/0360-3016(88)90060-0

Denman, D. L., Foster, A. E., Lewis, G. C., Jr., Redmond, K. P., Elson, H. R., Breneman, J. C., Kereiakes, J. G., & Aron, B. S. (1988b). The distribution of power and heat produced by interstitial microwave antenna arrays: II. The role of antenna spacing and insertion depth. International Journal of

Radiation Oncology, Biology, Physics, 14(3), 537-545. https://doi.org/10.1016/0360-3016(88)90271-4

Desouky, A. F., Abd El-Hameed, A. S., Eldamak, A. R., Abouelnaga, T. G., & Elhenawy, H. M. (2026). Dual-polarized Ku-band microstrip antenna array with metamaterial loading and protective superstrate for GB-SAR applications. Scientific Reports, 16, Article 14685. https://doi.org/10.1038/s41598-026-49752-0

Diao, Y., & Hirata, A. (2023). FDTD assessment of exposures to far-field mmWave beams in anatomical head model. IEEE Transactions on Electromagnetic Compatibility, 65(5), 1282–1291. https://doi.org/10.1109/TEMC.2023.3289450

Du, Y., Lu, M., & Xie, G. (2025). Dosimetric analysis of electromagnetic exposure by millimeter-wave 5G antenna arrays. Journal of Radiation Research and Radiation Processing, 43(6), Article 060501. https://doi.org/10.11889/j.1000-3436.2025-0040

Elkayal, H. A., Aly, M. H., & Ismail, N. E. (2024). Optimization of antenna excitations for non-invasive microwave hyperthermia for breast cancer treatment. Journal of Advanced Research in Applied Sciences and Engineering Technology, 39(2), 258–269. https://doi.org/10.37934/araset.39.2.258269

Fan, K., Huang, K., Xiao, Q., Wang, S., Liu, H., & Wang, H. (2025). Optimization design of spaceborne microstrip array by strain compensation method based on multi-physics coupling analysis. Electronics, 14(21), Article 4255. https://doi.org/10.3390/electronics14214255

Feresidis, A. P., & Vardaxoglou, J. C. (2001). High gain planar antenna using optimised partially reflective surfaces. IEE Proceedings—Microwaves, Antennas and Propagation, 148(6), 345–350. https://doi.org/10.1049/ip-map:20010828

Funahashi, D., Hirata, A., Kodera, S., & Foster, K. R. (2018). Area-averaged transmitted power density at skin surface as metric to estimate surface temperature elevation. IEEE Access, 6, 77665–77674. https://doi.org/10.1109/ACCESS.2018.2883733

Funahashi, D., Ito, T., Hirata, A., Iyama, T., & Onishi, T. (2018). Averaging area of incident power density for human exposure from patch antenna arrays. IEICE Transactions on Electronics, E101.C(8), 644–646. https://doi.org/10.1587/transele.E101.C.644

Gabriel, S., Lau, R. W., & Gabriel, C. (1996). The dielectric properties of biological tissues: III. Parametric models for the dielectric spectrum of tissues. Physics

in Medicine & Biology, 41(11), 2271–2293. https://doi.org/10.1088/0031-9155/41/11/003

Ge, L., Chen, L., He, P., Lin, H., Ruan, S., Qian, Z., & Mao, J. (2025). A novel system in antenna (SiA) with integrated RF circuits and thermal management. IEEE Transactions on Antennas and Propagation, 73(10), 7399–7408. https://doi.org/10.1109/TAP.2025.3585294

Haddaway, N. R., Grainger, M. J., & Gray, C. T. (2022). Citationchaser: A tool for transparent and efficient forward and backward citation chasing in systematic searching. Research Synthesis Methods, 13(4), 533–545. https://doi.org/10.1002/jrsm.1563

Haddaway, N. R., Page, M. J., Pritchard, C. C., & McGuinness, L. A. (2022). PRISMA2020: An R package and Shiny app for producing PRISMA 2020-compliant flow diagrams, with interactivity for optimised digital transparency and Open Synthesis. Campbell Systematic Reviews, 18(2), Article e1230. https://doi.org/10.1002/cl2.1230

He, W., Xu, B., Gustafsson, M., Ying, Z., & He, S. (2018). RF compliance study of temperature elevation in human head model around 28 GHz for 5G user equipment application: Simulation analysis. IEEE Access, 6, 830–838. https://doi.org/10.1109/ACCESS.2017.2776145

Hirata, A., Kodera, S., Sasaki, K., Gomez-Tames, J., Laakso, I., Wood, A., Watanabe, S., & Foster, K. R. (2021). Human exposure to radiofrequency energy above 6 GHz: Review of computational dosimetry studies. Physics in Medicine & Biology, 66(8), Article 08TR01. https://doi.org/10.1088/1361-6560/abf1b7

Jia, Z., Zhang, H., Yao, H., Wu, B., Liu, Y., & Liang, J. (2025). ETC-Net: Electromagnetic-thermal co-simulation network for microstrip patch antenna arrays inspired by mutiphysics chain-of-thought. Engineering Analysis with Boundary Elements, 179, Article 106324. https://doi.org/10.1016/j.enganabound.2025.106324

Kang, Z. Y., He, L., Pan, S., Fei, D., & Liang, G. (2026). Low-profile dual-CP antenna array using spiral sequential rotation technique for satellite communication. International Journal of Microwave and Wireless Technologies, 17(10), 1865–1874. https://doi.org/10.1017/S175907872510281X

Karniadakis, G. E., Kevrekidis, I. G., Lu, L., Perdikaris, P., Wang, S., & Yang, L. (2021). Physics-informed machine learning. Nature Reviews Physics, 3(6), 422–440. https://doi.org/10.1038/s42254-021-00314-5

Kim, S.-W., Yu, H.-G., & Choi, D.-Y. (2021). Analysis of patch antenna with broadband using octagon parasitic patch. Sensors, 21(14), Article 4908. https://doi.org/10.3390/s21144908

Kirinčić, M., Fadiga, T., & Delač, B. (2025). Influence of fin spacing and fin height in passive heat sinks: Numerical analysis with experimental comparison. Applied Sciences, 15(21), Article 11410. https://doi.org/10.3390/app152111410

Kour, H., Jha, R. K., & Jain, S. (2023). Antenna model for safe human exposure in future 6G smartphones: A network perspective. IEEE Transactions on Green Communications and Networking, 7(4), 2010–2024. https://doi.org/10.1109/TGCN.2023.3303471

Lee, K.-J., Oh, J., & Yi, S.-H. (2018). Stacked microstrip patch antenna array with high-gain and improved thermal-stability for microwave power transmission applications. 2018 Asia-Pacific Microwave Conference (APMC), 1432–1434. IEEE. https://doi.org/10.23919/APMC.2018.8617391

Li, P., Li, R., Fan, Z., Han, J., Ding, G., Wang, Q., Xu, W., & Rocca, P. (2026). 3D printed high-temperature ceramic conformal array antenna: Design, analysis, manufacturing, and testing. Defence Technology, 55, 340–353. https://doi.org/10.1016/j.dt.2025.05.012

Li, R., Li, P., Rocca, P., Salas Sánchez, A. Á., Song, L., Li, X., Xu, W., & Fan, Z. (2023). Design of wideband high-gain patch antenna array for high-temperature applications. Sensors, 23(8), Article 3821. https://doi.org/10.3390/s23083821

Liu, R., Mitchell, G. A., Johnson, W. J. D., Mumcu, G., & Wang, J. (2026). Mm-wave 3-D-printed 2 × 2 antenna subarray with structurally packaged beamforming IC and thermal management. IEEE Transactions on Components, Packaging and Manufacturing Technology, 16(2), 398–412. https://doi.org/10.1109/TCPMT.2025.3621409

Liu, Y., Zhang, S., & Gao, Y. (2017). A high-temperature stable antenna array for the satellite navigation system. IEEE Antennas and Wireless Propagation Letters, 16, 1397–1400. https://doi.org/10.1109/LAWP.2016.2639068

McGowan, J., Sampson, M., Salzwedel, D. M., Cogo, E., Foerster, V., & Lefebvre, C. (2016). PRESS peer review of electronic search strategies: 2015 guideline statement. Journal of Clinical Epidemiology, 75, 40–46. https://doi.org/10.1016/j.jclinepi.2016.01.021

Mechling, J. A., Strohbehn, J. W., & Ryan, T. P. (1992). Three-dimensional theoretical temperature distributions produced by 915 MHz dipole antenna arrays with varying insertion depths in muscle tissue. International Journal

of Radiation Oncology, Biology, Physics, 22(1), 131-138. https://doi.org/10.1016/0360-3016(92)90992-Q

Melouki, N., Hocini, A., Fegriche, F. Z., PourMohammadi, P., Naseri, H., Iqbal, A., & Denidni, T. A. (2022). High-gain wideband circularly polarised Fabry–Perot resonator array antenna using a single-layered pixelated PRS for millimetre-wave applications. Micromachines, 13(10), Article 1658. https://doi.org/10.3390/mi13101658

Mernyei, F., & Voelgyi, F. (1990). Simple methods for testing the temperature dependence of microstrip antenna arrays. 20th European Microwave Conference, 365–370. IEEE. https://doi.org/10.1109/euma.1990.336070

Miura, N., Kodera, S., Diao, Y., Higashiyama, J., Suzuki, Y., & Hirata, A. (2021). Power absorption and skin temperature rise from simultaneous near-field exposure at 2 and 28 GHz. IEEE Access, 9, 152140–152149. https://doi.org/10.1109/ACCESS.2021.3126372

Morelli, M. S., Gallucci, S., Siervo, B., & Hartwig, V. (2021). Numerical analysis of electromagnetic field exposure from 5G mobile communications at 28 GHz in adults and children users for real-world exposure scenarios. International Journal of Environmental Research and Public Health, 18(3), Article 1073. https://doi.org/10.3390/ijerph18031073

Munn, Z., Peters, M. D. J., Stern, C., Tufanaru, C., McArthur, A., & Aromataris, E. (2018). Systematic review or scoping review? Guidance for authors when choosing between a systematic or scoping review approach. BMC Medical Research Methodology, 18, Article 143. https://doi.org/10.1186/s12874-018-0611-x

Muzaffar, K., Roy, D., Tuli, S., & Koul, S. (2019). Frequency modulated thermal wave imaging for visualizing power density of electromagnetic waves on plane surfaces. Research in Nondestructive Evaluation, 30(2), 65–79. https://doi.org/10.1080/09349847.2017.1361492

Myllymäki, S., Sonkki, M., Kokkonen, M., Ghavidel, A., Ohsato, H., & Jantunen, H. (2022). Thermoplastic laminate and cordierite/indialite glass-ceramic hybrid package for 15-GHz operated antennas. IEEE Transactions on Components, Packaging and Manufacturing Technology, 12(4), 700–703. https://doi.org/10.1109/TCPMT.2022.3163557

Nagy, L. (2023). Microstrip antenna development for radar sensor. Sensors, 23(2), Article 909. https://doi.org/10.3390/s23020909

Neufeld, E., Carrasco, E., Murbach, M., Balzano, Q., Christ, A., & Kuster, N. (2018). Theoretical and numerical assessment of maximally allowable power-density averaging area for conservative electromagnetic exposure

assessment above 6 GHz. Bioelectromagnetics, 39(8), 617–630. https://doi.org/10.1002/bem.22147

Page, M. J., McKenzie, J. E., Bossuyt, P. M., Boutron, I., Hoffmann, T. C., Mulrow, C. D., Shamseer, L., Tetzlaff, J. M., Akl, E. A., Brennan, S. E., Chou, R., Glanville, J., Grimshaw, J. M., Hróbjartsson, A., Lalu, M. M., Li, T., Loder, E. W., Mayo-Wilson, E., McDonald, S., …, Moher, D. (2021). The PRISMA 2020 statement: An updated guideline for reporting systematic reviews. BMJ, 372, Article n71. https://doi.org/10.1136/bmj.n71

Park, J., Kim, D., Kim, H., Lee, J., & Chung, W. (2021). Thermal radiative copper oxide layer for enhancing heat dissipation of metal surface. Nanomaterials, 11(11), Article 2819. https://doi.org/10.3390/nano11112819

Pascawati, A., Fakhri, M., Wahdiyat, A. I., Putro, I. E., Harsono, S. D., Rahmat, M. Z., Duhri, R. A., Rahardiyanti, K., Irwanto, H. Y., Wahyu, Y., Rufiyanto, A., Sulistya, B., Qomariya, E. N., Rahayu, C. R., Ridho, R. F., & Aziz, M. R. K. (2024). Conformal microstrip antennas on the rocket cylinder. Progress In Electromagnetics Research M, 126, 1–10. https://doi.org/10.2528/PIERM23103104

Patel, H., Liu, R., Wang, J., & Mumcu, G. (2026). Compact mm-wave antenna arrays with structurally integrated active devices. 2026 IEEE International Symposium on Antennas and Propagation and USNC-URSI Radio Science Meeting, 150–153. IEEE. https://doi.org/10.1109/AP-S/USNC-URSI60190.2026.11675179

Peters, M. D. J., Godfrey, C., McInerney, P., Khalil, H., Larsen, P., Marnie, C., Pollock, D., Tricco, A. C., & Munn, Z. (2022). Best practice guidance and reporting items for the development of scoping review protocols. JBI Evidence Synthesis, 20(4), 953–968. https://doi.org/10.11124/JBIES-21-00242

Peters, M. D. J., Marnie, C., Tricco, A. C., Pollock, D., Munn, Z., Alexander, L., McInerney, P., Godfrey, C. M., & Khalil, H. (2020). Updated methodological guidance for the conduct of scoping reviews. JBI Evidence Synthesis, 18(10), 2119–2126. https://doi.org/10.11124/JBIES-20-00167

Pollock, D., Peters, M. D. J., Khalil, H., McInerney, P., Alexander, L., Tricco, A. C., Evans, C., de Moraes, É. B., Godfrey, C. M., Pieper, D., Saran, A., Stern, C., & Munn, Z. (2023). Recommendations for the extraction, analysis, and presentation of results in scoping reviews. JBI Evidence Synthesis, 21(3), 520–532. https://doi.org/10.11124/JBIES-22-00123

Pop, E., Varshney, V., & Roy, A. K. (2012). Thermal properties of graphene: Fundamentals and applications. MRS Bulletin, 37(12), 1273–1281. https://doi.org/10.1557/mrs.2012.203

Pramono, S., Sumantyo, J. T. S., Ibrahim, M. H., Takahashi, A., Yoshimoto, Y., Kashihara, H., Santosa, C. E., Gao, S., & Ito, K. (2025). A novel low temperature cofired-cordierite ceramic substrate-based compact ultra-wideband circularly polarized array antenna for C-band remote sensing application. IEEE Open Journal of Antennas and Propagation, 6(3), 715–725. https://doi.org/10.1109/OJAP.2025.3544279

Raissi, M., Perdikaris, P., & Karniadakis, G. E. (2019). Physics-informed neural networks: A deep learning framework for solving forward and inverse problems involving nonlinear partial differential equations. Journal of Computational Physics, 378, 686–707. https://doi.org/10.1016/j.jcp.2018.10.045

Rani, S., Marwaha, A., & Marwaha, S. (2020). Investigation of substrate materials for graphene oxide absorber loaded antenna array increased ambient temperature. Photonic Network Communications, 40(2), 94–102. https://doi.org/10.1007/s11107-020-00908-6

Rao, K. P., Vani, R. M., & Hunagund, P. V. (2018). Planar microstrip patch antenna array with gain enhancement. Procedia Computer Science, 143, 48-57. https://doi.org/10.1016/j.procs.2018.10.350

Rethlefsen, M. L., Kirtley, S., Waffenschmidt, S., Ayala, A. P., Moher, D., Page, M. J., Koffel, J. B., & PRISMA-S Group (2021). PRISMA-S: An extension to the PRISMA statement for reporting literature searches in systematic reviews. Systematic Reviews, 10, Article 39. https://doi.org/10.1186/s13643-020-01542-z

Sacco, G., Pisa, S., & Zhadobov, M. (2021). Age-dependence of electromagnetic power and heat deposition in near-surface tissues in emerging 5G bands. Scientific Reports, 11, Article 3983. https://doi.org/10.1038/s41598-021-82458-z

Sasaki, K., Porter, E., Rashed, E. A., Farrugia, L., & Schmid, G. (2022). Measurement and image-based estimation of dielectric properties of biological tissues—past, present, and future—. Physics in Medicine & Biology, 67(14), Article 14TR01. https://doi.org/10.1088/1361-6560/ac7b64

Shahil, K. M. F., & Balandin, A. A. (2012). Graphene–multilayer graphene nanocomposites as highly efficient thermal interface materials. Nano Letters, 12(2), 861–867. https://doi.org/10.1021/nl203906r

Sheng, X., Lu, X., Liu, N., & Liu, Y. (2022). Design of broadband high-gain Fabry–Pérot antenna using frequency-selective surface. Sensors, 22(24), Article 9698. https://doi.org/10.3390/s22249698

Simone, M., Lodi, M. B., Curreli, N., Pavone, S. C., Mazzarella, G., & Fanti, A. (2021). Optimized design and multiphysics analysis of a Ka-band stacked

antenna for CubeSat applications. IEEE Journal on Multiscale and Multiphysics Computational Techniques, 6, 143–157. https://doi.org/10.1109/JMMCT.2021.3115702

Song, R., Zhao, X., Wang, Z., Fu, H., Han, K., Qian, W., Wang, S., Shen, J., Mao, B., & He, D. (2020). Sandwiched graphene clad laminate: A binder-free flexible printed circuit board for 5G antenna application. Advanced Engineering Materials, 22(10), Article 2000451. https://doi.org/10.1002/adem.202000451

Straume, A., Oftedal, G., & Johnsson, A. (2005). Skin temperature increase caused by a mobile phone: A methodological infrared camera study. Bioelectromagnetics, 26(6), 510–519. https://doi.org/10.1002/bem.20124

Suseela, S., & Wahid, P. (2020). Breast cancer hyperthermia using a grid array applicator. SoutheastCon 2020, Article 9249686. IEEE. https://doi.org/10.1109/SoutheastCon44009.2020.9249686

Tricco, A. C., Lillie, E., Zarin, W., O'Brien, K. K., Colquhoun, H., Levac, D., Moher, D., Peters, M. D. J., Horsley, T., Weeks, L., Hempel, S., Akl, E. A., Chang, C., McGowan, J., Stewart, L., Hartling, L., Aldcroft, A., Wilson, M. G., Garritty, C., …, Straus, S. E. (2018). PRISMA extension for scoping reviews (PRISMA-ScR): Checklist and explanation. Annals of Internal Medicine, 169(7), 467–473. https://doi.org/10.7326/M18-0850

Underwood, H. R., Peterson, A. F., & Magin, R. L. (1992). Electric-field distribution near rectangular microstrip radiators for hyperthermia heating: Theory versus experiment in water. IEEE Transactions on Biomedical Engineering, 39(2), 146–153. https://doi.org/10.1109/10.121645

van den Akker, O. R., Peters, G.-J. Y., Bakker, C. J., Carlsson, R., Coles, N. A., Corker, K. S., Feldman, G., Moreau, D., Nordström, T., Pickering, J. S., Riegelman, A., Topor, M. K., van Veggel, N., Yeung, S. K., Call, M., Mellor, D. T., & Pfeiffer, N. (2023). Increasing the transparency of systematic reviews: Presenting a generalized registration form. Systematic Reviews, 12, Article 170. https://doi.org/10.1186/s13643-023-02281-7

Vencels, J., Birjukovs, M., Kataja, J., & Råback, P. (2019). Microwave heating of water in a rectangular waveguide: Validating EOF-Library against COMSOL multiphysics and existing numerical studies. Case Studies in Thermal Engineering, 15, Article 100530. https://doi.org/10.1016/j.csite.2019.100530

Wang, H., Luo, K., Li, E., Tang, B., & Yuan, Y. (2026). Interfacial engineering enables low-loss and thermally stable bismaleimide-triazine composites for high-frequency packaging and substrate applications. Applied Surface Science, 732, Article 166569. https://doi.org/10.1016/j.apsusc.2026.166569

Wang, W., Bao, J., Wang, C., He, G., Wang, X., Xu, D., Jin, B., Shi, Z., Darwish, M. A., Chen, Y., Liang, Q., Zhang, M., & Zhou, D. (2025). LiMSiO4 (M = Ga, Sc and Y): Low-permittivity and high thermal conductivity microwave dielectric ceramics for millimeter-wave communications. Journal of Materials Science and Technology, 225, 288–296. https://doi.org/10.1016/j.jmst.2024.12.004

Xia, H., Liu, Z., Liu, H., Zhang, T., Wang, F., Hu, X., Wu, X., Li, L., & Wang, Z. (2023). A cost-effective wideband dual-polarized L-shaped probe-fed phased array antenna for 60-GHz AiP applications. IEEE Transactions on Components, Packaging and Manufacturing Technology, 13(11), 1790–1803. https://doi.org/10.1109/TCPMT.2023.3319035

Xia, Y., Liu, N., Yang, Z., Liu, Y., Sheng, X., Zhang, D., Jiang, G., & Li, X. (2026). Research on microstrip array antennas for microwave de-icing of wind turbine blades. Progress in Electromagnetics Research C, 164, 89–95. https://doi.org/10.2528/PIERC25081902

Xiao, H., Zhu, W., Wang, Y., & He, L. (2025). Optimizing microwave-sensitive coatings for enhanced de-icing efficiency: Effects of frequency, antenna design, and surface geometry. Science Progress, 108(3), Article 00368504251366370. https://doi.org/10.1177/00368504251366370

Xu, F., & Zhang, X. (2025). A high-temperature stabilized anti-interference Beidou array antenna. Electronics, 14(8), Article 1555. https://doi.org/10.3390/electronics14081555

Xu, Y., Feng, Y., Chao, J., Zhang, H., Liu, Y., Li, X., Tang, W., & Zhang, G. (2023). A wideband dual-polarized base station antenna with heat dissipation function based on PIN structure. IEEE Transactions on Vehicular Technology, 72(9), 11924–11934. https://doi.org/10.1109/TVT.2023.3270842

Yee, K. S. (1966). Numerical solution of initial boundary value problems involving Maxwell's equations in isotropic media. IEEE Transactions on Antennas and Propagation, 14(3), 302–307. https://doi.org/10.1109/TAP.1966.1138693

Yoo, J., Lee, M. L., & Yang, Y. S. (2025). 3D printed and circularly polarized 28 GHz patch antenna array for small satellite communications. Aerospace Science and Technology, 164, Article 110443. https://doi.org/10.1016/j.ast.2025.110443

Zeng, X., Huang, K., Hu, Z., Chen, Q., & Xiao, W. (2017). A circularly polarized HTS microstrip antenna array with controllable cryostat. International Journal of Antennas and Propagation, 2017, Article 6035202. https://doi.org/10.1155/2017/6035202

Zhang, B., Fan, K., Chen, J., & Wu, S. (2026). A conformal antenna array with small-sized focal spots for hyperthermia. IEEE Transactions on Antennas and Propagation, 74(2), 2137–2142. https://doi.org/10.1109/TAP.2025.3636181

Zhao, Z., Zhu, Z.-C., You, B., Chen, X.-P., Xu, Z.-R., Wu, L.-S., & Mao, J.-F. (2025). A K-band fully-integrated multi-channel active antenna-in-package module in low-temperature cofired ceramic. IEEE Transactions on Antennas and Propagation, 73(7), 4957–4962. https://doi.org/10.1109/TAP.2025.3550452

Zhou, J., Yin, L., Kang, L., Wang, M., & Huang, J. (2019). Joint design and experimental tests of highly integrated phased-array antenna with microchannel heat sinks. IEEE Antennas and Wireless Propagation Letters, 18(11), 2370–2374. https://doi.org/10.1109/LAWP.2019.2914495